IEEE Access
Multidisciplinary | Rapid Review | Open Access Journal

SPECIAL SECTION ON EMERGING TECHNOLOGIES FOR DEVICE TO DEVICE COMMUNICATIONS

Received October 7, 2018, accepted October 18, 2018, date of publication October 23, 2018,
date of current version November 19, 2018.

Digital Object Identifier 10.1109/ACCESS.2018.2877638

Force and Moment Compensation Method Based on Three Degree-of-Freedom Stiffness-Damping Identification for Manipulator Docking Hardware-In-The-Loop Simulation System

SIMIAO YU[1], JUNWEI HAN[1], YU YANG[1], DONGMEI XU[2], AND ZHIYONG QU[1]
[1]School of Mechatronics Engineering, Harbin Institute of Technology, Harbin 150001, China
[2]School of Mechanical Engineering, Xi'an University of Science and Technology, Xi'an 710054, China

Corresponding author: Yu Yang (yangyu1980hit@163.com)

This work was supported by the National Natural Science Foundation of China under Grant 51475116 and Grant 51505100.

ABSTRACT The space manipulator docking hardware-in-the-loop (HIL) simulation system is an important means to simulate the real space docking on the ground. In this paper, a space manipulator docking HIL system is designed, the space manipulator docking dynamics model is established and the motion process of space docking is simulated by a six degree-of-freedom (DOF) parallel robot. Delays exist in the force sensor and the parallel robot of the HIL system and are unavoidable; which not only affect the accuracy of the HIL system simulation, but also lead to instability of the system, resulting in docking failure and damage to the docking mechanism (DM). In view of the contact characteristics of DM, a force and moment compensation method based on three DOF stiffness-damping identification is proposed in this paper. Considering the time-varying characteristics of multi-DOF contact parameters, on-line identification is applied to identify the stiffness and damping in three perpendicular directions. Then a six DOF compensation model is established to compensate the deviation of contact force and moment caused by the delays, so as to improve the stability and reproduction accuracy of the system. Compared with the existing single DOF compensation researches, the considering of contact parameters and the model of compensation in this paper are all applicable to multi-DOF system. Moreover, the compensation model doesn't need the model and delay characteristics of the parallel robot, so it is a model-free compensation. The effectiveness of the proposed compensation method is verified by simulation and experiment.

INDEX TERMS Manipulator docking, hardware-in-the-loop simulation system, docking dynamics, three DOF stiffness-damping identification, force and moment compensation.

I. INTRODUCTION

The research on the ground simulation technology of the space manipulator docking is particularly important with the development of the space exploration. The manipulator's terminal is equipped with an end-effector that uses a DM to achieve capture, drag and other docking operations on a target-adapter equipped on the spacecraft. Due to the high cost and important tasks, docking characteristics of manipulators with different stiffness, capture ability of the DM and docking strategy must be verified on the ground before the spacecraft launch to ensure the success of the real docking. Thus, accurate simulation of the docking dynamics process on the ground is of great significance for the design of the DM, the manipulator in orbit service and the space station construction [1]–[3].

The HIL simulation is frequently used because it reduces cost and ensures simulation fidelity with flexibility on changing flying objects. The docking simulation process of the space manipulator is carried out under zero gravity (zero-g) condition to simulate the weightless state of real space [4], [5]. At present, the simulation object of space docking HIL simulation system is usually two rigid spacecrafts docking; the motion of spacecraft in zero-g space is usually computed from a dynamics model; and the motion process of the spacecraft is simulated through the robot, such as in [6]–[8]. The mechanical composition and dynamics model of the

space manipulator docking are more complicated. The DM used in the space manipulator docking HIL simulation system in this study is the same as that in real space; the motions of the spacecraft, the manipulator and the space station in the zero-g space are calculated by the dynamics model; and the relative motion of the mechanisms is reproduced by the parallel robot. The involvement of the manipulator makes the system dynamics model complex; since the joints are locked during the docking process to eliminate the adverse effect of large range motion at the end of the manipulator on the docking [9]. The motion state of the manipulator during the docking process is represented as elastic deformation. When reproducing the fundamental frequency characteristics of the manipulator motion, the manipulator can be equivalent to a six DOF mass-stiffness-damping system. This modeling method can simplify the complex manipulator model and more intuitively study the docking characteristics of manipulators with different stiffness.

In addition to dynamics, one of the most challenging problems for the HIL simulation is divergence and accuracy loss. The dynamic response delay of the six DOF parallel robot causes that the actual position of the motion deviates from the desired position of the dynamics calculation, resulting in the actual force and moment (the force and moment input to the dynamics calculation model) measured by the sensor deviate from the desired force and moment corresponding to the desired position, which called the force and moment delay. After cyclic calculation and measurement, the error accumulations of parallel robot's displacement and measurement force increase, which not only affect the system reproduction accuracy, but also cause the system divergence. Thus, the delay compensation is very important for the manipulator docking HIL simulation.

Some literatures have studied of the delay problem of HIL simulation systems. Zebenay *et al.* [10]. established the serial robot model as the second-order delay system, and the critical delay and associated frequency were derived as a function of the satellites' mass, the contact stiffness and damping parameters, then the value relation of indexes which satisfied the stability was obtained by using pole location method. In [11] and [12], the parallel robot was established as a third-order delay system, docking HIL simulation system model of two rigid spacecrafts was established, and the stability conditions and the dynamic frequency range which can be simulated of the system were obtained; however, there was no compensation for delay in the literatures. Chang *et al.* [13] considered the delay of electrical components and digital control, and developed a compensate model based on the quantitative feedback theory. Shimoji *et al.* [14] applied a first-order compensation model aiming at the pure or first-order time delay, which decreased the delay of the simulator. Osaki *et al.* [15] and Abiko *et al.* [16] used compensated force methods to achieve the expected contact force by adding the virtual force onto the measurement force. But the delay models in the literatures are known; when the delay model is unknown, the compensation method becomes difficult and immature. Ananthakrishnan *et al.* [17] developed a prediction-based feed forward filter to make a ground-based hydraulic simulator generate contact forces and rebound velocities that matched those expected during shuttle on-orbit; however, the prediction model was trained offline, the on-orbit data for the training was unknown before the simulation. Zebenay *et al.* [10] used the virtual damper force to compensate the measurement force; although the delay model of the simulator was not required, this method required a large number of experiments and experience to modify the model and parameters. Qi *et al.* [18] studied the force compensation for the system delay in the form of elastic contact collision, the measurement force was compensated by identifying the stiffness, and the stability of the system was improved. Yu *et al.* [19] proposed a hybrid force and displacement compensation method based on on-line identification to compensate the delayed force of a space docking HIL simulation system with multi-stiffness, multi-damping and single mass; and good stability was obtained. The methods presented in these literatures can improve the performance of systems with unknown delay models, but they are all based on the studies of single DOF, and the research objects are based on docking systems of two rigid spacecrafts.

The delay of the parallel robot is unavoidable and the delay characteristics are different at different positions; meanwhile, the space manipulator docking is multi-DOF motion and the contact environment parameters are time-varying. The compensation and correction method for the dynamic response delay of the parallel robot or the contact force delay by prediction and experiment is tedious and prone to deviation. In this paper, according to the contact form of the DM, a force and moment compensation method based on three DOF stiffness-damping on-line identification is proposed to prevent the divergence of the space manipulator docking HIL simulation system and to improve the reproduction accuracy of the system. The main contributions of this paper are as follows:

1) The research object is different: in this study the research object is the docking process of space manipulator, the HIL simulation system of the space manipulator docking is designed, and the docking dynamics model of space manipulator is established;

2) The motion of the research object is multi-DOF, and the contact environment parameters are time-varying;

3) According to the contact characteristics of the DM, the contact forces in three directions are considered as elastic forces determined by stiffness and damping in three directions. A force and moment compensation method based on on-line identification of three DOF stiffness-damping is proposed to ensure that the force and moment input to the dynamics model at any time is the same as the desired force and moment corresponding to the desired position. In addition, the compensation method is model-free compensation.

This paper consists of six sections. Following this section of the introduction, the HIL simulation system for

manipulator docking is introduced in Section 2. The model of the manipulator docking HIL simulation system is described in Section 3. Compensation models of HIL simulation system for manipulator docking are proposed in Section 4. Simulations and experiments are included in Section 5. Finally, Section 6 gives the conclusion.

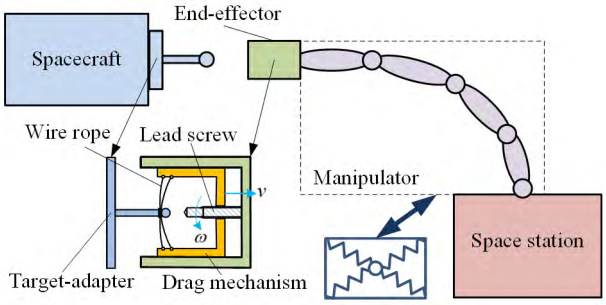

FIGURE 1. The space manipulator docking system.

II. HIL SIMULATION SYSTEM FOR MANIPULATOR DOCKING

A. MANIPULATOR DOCKING SYSTEM

The space manipulator docking system, as shown in Fig. 1, consists of a spacecraft, a manipulator, an end-effector and a space station. To describe the elastic deformation and elastic force of the manipulator, the manipulator is equivalent to a six DOF spring damping system, and the mass characteristics of the manipulator are equivalent to the terminal of the end-effector. The end-effector moves with the action of the six DOF spring damping system and the contact force. During the docking, the drag mechanism in the end-effector fixes and drags the butt rod of the target-adapter and makes the spacecraft move. Schematic diagram of the DM and the drag principle is shown in Fig. 1. A lead screw is mounted inside the end-effector, and motor drives the lead screw to rotate at a constant angular velocity; the constant velocity rotation of the lead screw can be transformed into a constant velocity linear motion of the DM. The DM captures and fixes the butt rod of the target-adapter through three wire ropes and then drives the target-adapter.

B. HIL SIMULATION SYSTEM FOR MANIPULATOR DOCKING

The structure of the HIL simulation system for manipulator docking is illustrated in Fig. 2. The physical objects include a force sensor, an end-effector, a six DOF parallel robot, a target-adapter (installed on the six DOF parallel robot) and a frame. The target-adapter and the end-effector used in the HIL simulation are the same as those in real space, which generate an actual contact force during the contact. The force sensor is attached under the frame and the end-effector is installed under the force sensor so that the force sensor can directly measure the impact force and moment when docking. The dynamics model used in the HIL simulation describes the

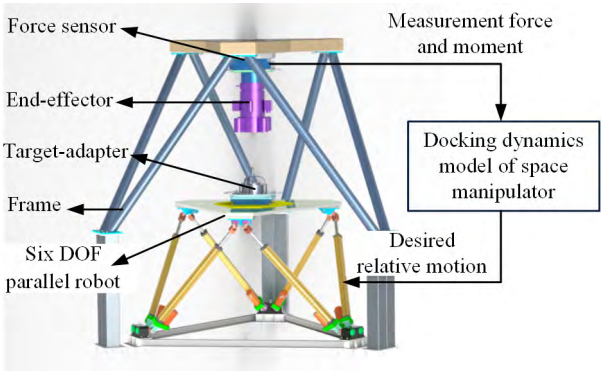

FIGURE 2. Structure of the HIL simulation system for manipulator docking.

motion in zero-g space of the mechanisms. The docking state depends on the relative position of the DM (target-adapter and end-effector). Thus the relative position parameters of the spacecraft and the end-effector are solved by the dynamics model, and the relative motion process is reproduced by the parallel robot.

In this study, the dynamics calculation of space manipulator docking and the control of the six DOF parallel robot are accomplished by two sets of upper and lower computers. The upper and lower computers transmit data through Ethernet, and two lower computers transmit data through reflective memory. The lower computer for dynamics calculation receives the measurement force, calculates the displacement and transfers it to the parallel robot control lower computer. The parallel robot control lower computer, the control component and the parallel robot driving component make up the position control system, and realize the closed-loop control of the parallel robot.

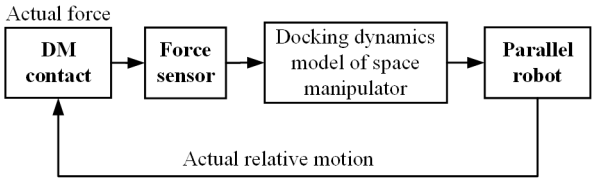

FIGURE 3. The principle of the HIL simulation for manipulator docking.

C. PRINCIPLE OF THE HIL SIMULATION SYSTEM FOR MANIPULATOR DOCKING

The principle of the HIL simulation for manipulator docking is shown in Fig. 3. The physical elements of Fig. 3 are in bold words, and the software model of Fig. 3 is in non-bold words. The force sensor determines whether the HIL system can get actual contact force at the current moment, and the parallel robot determines whether the HIL system can reproduce the desired displacement to get the desired contact force at the next moment. When the docking dynamics model can accurately describe the motion of the mechanisms; the smaller the delays of the force sensor and the parallel robot are, the

closer the HIL simulation system is to the real space docking. If the force sensor and the parallel robot can transmit force and motion one-to-one, the HIL simulation system can be considered to accurately reproduce the real space docking process.

III. MODELING OF THE HIL SIMULATION SYSTEM FOR MANIPULATOR DOCKING

Based on the principle of the HIL simulation for manipulator docking, the space manipulator docking HIL simulation system model consists of docking dynamics model, parallel robot model, force sensor model and DM contact model.

A. DOCKING DYNAMICS MODEL OF SPACE MANIPULATOR

Docking dynamics model of the space manipulator is used to solve the motion state of the end-effector, the space manipulator, the space station and the spacecraft under the action of the contact force and moment (measured by the sensor), and finally the relative motion of the spacecraft and the end-effector is obtained.

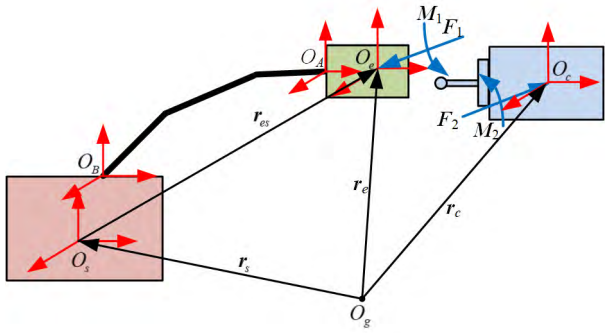

FIGURE 4. Force diagram of the space manipulator docking.

The force of the DM is shown in Fig. 4. Define the following coordinate systems for establish mathematical models: $O_gX_gY_gZ_g$—Inertial coordinate system; $O_eX_eY_eZ_e$—End-effector body-fixed coordinate system, the coordinate origin locates at the comprehensive centroid of the end-effector and manipulator (short for end-effector's centroid); $O_cX_cY_cZ_c$—Spacecraft body-fixed coordinate system, the coordinate origin locates at the centroid of the passive spacecraft; $O_sX_sY_sZ_s$—Space station body-fixed coordinate system, the coordinate origin locates at the centroid of the space station.O_A and O_B are the mounting positions of the manipulator on the end-effector and the space station, respectively. $O_BX_BY_BZ_B$—Stiffness and damping coordinate system, the directions of the principal stiffness and principle damping are the same as that of the directions of the coordinate axes, assume that the direction of $O_BX_BY_BZ_B$ is the same as that of the $O_sX_sY_sZ_s$. In addition, R_{mn} represents the coordinate transformation matrix from the coordinate system m to the coordinate system n; E_{mn} represents the transformation matrix from the body coordinate system's angular velocity of the coordinate system m relative to the coordinate system n to the Euler angular velocity.

The contact force acting on the end-effector is $\boldsymbol{F}_1$, the moment M_1 is generated by the contact force at the comprehensive centroid. The force and moment of the manipulator (six DOF spring damping system) generated by the deformation and torsion are $\boldsymbol{F}_h$ and $\boldsymbol{M}_h$, respectively. Newton equations of end-effector and space station in $O_gX_gY_gZ_g$ are:

$$\ddot{\boldsymbol{r}}_s = \frac{\boldsymbol{R}_{sg}\cdot\boldsymbol{F}_h}{m_s};\quad \ddot{\boldsymbol{r}}_e = \frac{-\boldsymbol{R}_{sg}\cdot\boldsymbol{F}_h+\boldsymbol{F}_1}{m_e} \tag{1}$$

where m_e indicates the comprehensive mass of end-effector and manipulator (short for the mass of the end-effector), m_s indicates the mass of space station, $\boldsymbol{r}_s$ indicates the position vector of space station's centroid in $O_gX_gY_gZ_g$, $\boldsymbol{r}_e$ indicates the position vector of end-effector's centroid in $O_gX_gY_gZ_g$.

Therefore, acceleration of end-effector relative to space station in $O_gX_gY_gZ_g$ is:

$$\boldsymbol{a}_{es} = \ddot{\boldsymbol{r}}_{es} = \frac{-\boldsymbol{R}_{sg}\cdot\boldsymbol{F}_h+\boldsymbol{F}_1}{m_e} - \frac{\boldsymbol{R}_{sg}\cdot\boldsymbol{F}_h}{m_s} \tag{2}$$

Relative acceleration of end-effector relative to space station $\dot{\boldsymbol{V}}_{es}$ in $O_sX_sY_sZ_s$ is:

$$\dot{\boldsymbol{V}}_{es} = \boldsymbol{a}_{es} - 2\boldsymbol{\omega}_s\times\boldsymbol{V}_{es} - \dot{\boldsymbol{\omega}}_s\times\boldsymbol{r}_{es} - \boldsymbol{\omega}_s\times(\boldsymbol{\omega}_s\times\boldsymbol{r}_{es}) \tag{3}$$

where ω_s is the angular velocity of the space station.

Relative velocity vector $\boldsymbol{V}_{es}$ and relative displacement vector $\boldsymbol{S}_{es}$ between two mechanisms in $O_sX_sY_sZ_s$ can be obtained by integrating the formula (3).

Rotation equations of end-effector and space station are as follows:

$$\boldsymbol{J}_s\cdot\boldsymbol{\varepsilon}_s + \boldsymbol{\omega}_s\times(\boldsymbol{J}_s\cdot\boldsymbol{\omega}_s) = \boldsymbol{r}_{As}\times\boldsymbol{F}_h + \boldsymbol{M}_h \tag{4}$$

$$\boldsymbol{J}_e\cdot\boldsymbol{\varepsilon}_e + \boldsymbol{\omega}_e\times(\boldsymbol{J}_e\cdot\boldsymbol{\omega}_e) = \boldsymbol{M}_1 - \boldsymbol{r}_{Ae}\times\left(\boldsymbol{R}_{es}^{-1}\cdot\boldsymbol{F}_h\right) - \boldsymbol{R}_{es}^{-1}\cdot\boldsymbol{M}_h \tag{5}$$

where $\boldsymbol{\varepsilon}_s$ and $\boldsymbol{\varepsilon}_e$ indicate the angular accelerations of the space station and the end-effector, respectively; $\boldsymbol{r}_{As}$ and $\boldsymbol{r}_{Ae}$ indicate the vectors of point O_A to the space station's centroid and to the end-effector's centroid, respectively; $\boldsymbol{J}_s$ indicates the inertia tensor of space station; $\boldsymbol{J}_e$ indicates comprehensive inertia tensor of the end-effector and manipulator (short for inertia tensor of the end-effector).

Angular velocity vector of end-effector relative to the space station is:

$$\boldsymbol{\omega}_{es} = \boldsymbol{\omega}_e - \boldsymbol{R}_{es}^{-1}\cdot\boldsymbol{\omega}_s \tag{6}$$

Euler-angle change rate of end-effector relative to the space station is:

$$\dot{\boldsymbol{\Phi}}_{es} = \boldsymbol{E}_{es}^{-1}\cdot\boldsymbol{\omega}_{es} \tag{7}$$

Euler-angle of the end-effector relative to the space station $\boldsymbol{\Phi}_{es}$ can be obtained by integrating the formula (7). The elastic deformation force $\boldsymbol{F}_h$ and the rotational moment $\boldsymbol{M}_h$ can be obtained by the stiffness, damping and deformation

of the manipulator. The two installation positions of the manipulator are on the end-effector and the space station, the relative rotational angles and relative angular velocities of the $O_AX_AY_AZ_A$ and $O_BX_BY_BZ_B$ at the two installation positions are the same as those of the end-effector and the space station, respectively, which are:

$$\begin{cases} \Delta\boldsymbol{\Phi}_{AB} = \boldsymbol{\Phi}_{es} \\ \Delta\dot{\boldsymbol{\Phi}}_{AB} = \dot{\boldsymbol{\Phi}}_{es} \end{cases} \tag{8}$$

The relative translational displacement and velocity of $O_AX_AY_AZ_A$ and $O_BX_BY_BZ_B$ are deduced as follows. The relative position of point O_A to point O_B in $O_sX_sY_sZ_s$ is:

$$\boldsymbol{r}_{AB} = \boldsymbol{S}_{es} - \boldsymbol{r}_{Bs} + \boldsymbol{R}_{es} \cdot \boldsymbol{r}_{Ae} \tag{9}$$

The change of relative translational motion at the manipulator's two installation positions is:

$$\Delta\boldsymbol{r}_{AB} = \boldsymbol{r}_{AB} - \boldsymbol{r}_{AB}(0) \tag{10}$$

The relative velocity of point O_A to point O_B in $O_sX_sY_sZ_s$ is:

$$\Delta\dot{\boldsymbol{r}}_{AB} = \boldsymbol{R}_{sg}^{-1} \cdot (\int \boldsymbol{a}_{es} \cdot dt + \boldsymbol{\omega}_e \cdot \boldsymbol{r}_{Ae} - \boldsymbol{\omega}_s \cdot \boldsymbol{r}_{es}) \tag{11}$$

The force and moment generated by manipulator (six DOF spring damping system) are:

$$\begin{bmatrix} \boldsymbol{F}_h \\ \boldsymbol{M}_h \end{bmatrix} = \boldsymbol{K} \cdot \begin{bmatrix} \Delta\boldsymbol{r}_{AB} \\ \Delta\boldsymbol{\Phi}_{AB} \end{bmatrix} + \boldsymbol{C} \cdot \begin{bmatrix} \Delta\dot{\boldsymbol{r}}_{AB} \\ \Delta\dot{\boldsymbol{\Phi}}_{AB} \end{bmatrix} \tag{12}$$

where $\boldsymbol{K}$ and $\boldsymbol{C}$ indicate the stiffness matrix and damping matrix of manipulator, respectively.

$\boldsymbol{K}$ and $\boldsymbol{C}$ can be measured or got by design value and analysis value. Motion parameters of the end-effector can be obtained by summarizing formula (1) to formula (12).

The force acting on the spacecraft is $\boldsymbol{F}_2$, acceleration of the spacecraft relative to the end-effector in $O_gX_gY_gZ_g$ is:

$$\boldsymbol{a}_{ce} = \ddot{\boldsymbol{r}}_{ce} = \frac{\boldsymbol{F}_2}{m_c} - \frac{-\boldsymbol{R}_{sg} \cdot \boldsymbol{F}_h + \boldsymbol{F}_1}{m_e} \tag{13}$$

where m_c indicates the mass of the spacecraft, $\boldsymbol{r}_c$ indicates the position vector of the spacecraft's centroid in $O_gX_gY_gZ_g$.

Relative acceleration of spacecraft relative to the end-effector $\dot{\boldsymbol{V}}_{\boldsymbol{ce}}$ in $O_eX_eY_eZ_e$ is:

$$\dot{\boldsymbol{V}}_{ce} = \boldsymbol{a}_{ce} - 2\boldsymbol{\omega}_e \times \boldsymbol{V}_{ce} - \dot{\boldsymbol{\omega}}_e \times \boldsymbol{r}_{ce} - \boldsymbol{\omega}_e \times (\boldsymbol{\omega}_e \times \boldsymbol{r}_{ce}) \tag{14}$$

Relative velocity vector $\boldsymbol{V}_{ce}$ and relative displacement vector $\boldsymbol{S}_{ce}$ between two mechanisms in $O_eX_eY_eZ_e$ can be obtained by integrating the formula (14).

The rotation modeling of the spacecraft is:

$$\boldsymbol{J}_c \cdot \boldsymbol{\varepsilon}_c + \boldsymbol{\omega}_c \times (\boldsymbol{J}_c \cdot \boldsymbol{\omega}_c) = \boldsymbol{M}_2 \tag{15}$$

where ε_c indicates the angular acceleration of the spacecraft; $\boldsymbol{M}_2$ is the moment generated by contact force at spacecraft centroid; $\boldsymbol{J}_c$ indicates the inertia tensor of the spacecraft.

Angular velocity vector of the spacecraft relative to the end-effector is:

$$\boldsymbol{\omega}_{ce} = \boldsymbol{\omega}_c - \boldsymbol{R}_{ce}^{-1} \cdot \boldsymbol{\omega}_e \tag{16}$$

Euler-angle change rate of the spacecraft relative to the end-effector is:

$$\dot{\boldsymbol{\Phi}}_{ce} = \boldsymbol{E}_{ce}^{-1} \cdot \boldsymbol{\omega}_{ce} \tag{17}$$

The Euler-angle of the spacecraft relative to the end-effector $\boldsymbol{\Phi}_{ce}$ can be obtained by integrating the formula (17). $\boldsymbol{S}_{ce}$ and $\boldsymbol{\Phi}_{ce}$ are the relative motion parameters that the parallel robot needs to simulate.

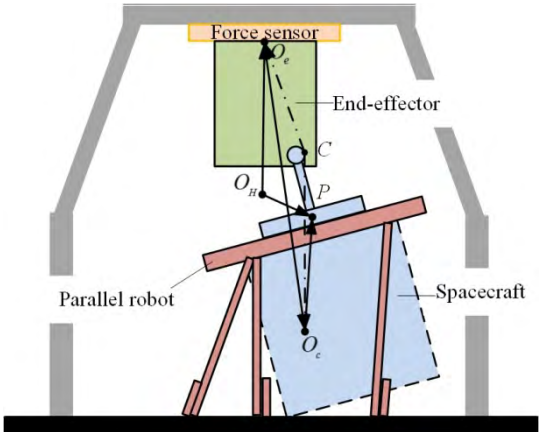

FIGURE 5. Sketch of parallel robot simulating relative motion.

B. PARALLEL ROBOT MODEL

The schematic diagram of the docking process reproducing by the parallel robot is shown in Fig. 5. To reduce the description of the coordinate system, assuming that the centroid coordinate system of the end-effector $O_eX_eY_eZ_e$ coincides with the measurement coordinate system of the force sensor, and then the force and moment measured by the sensor are the force and moment acting on the end-effector's centroid. The dotted line below the parallel robot platform in Fig. 5 is used to indicate a virtual spacecraft, and the target-adapter mounted on the spacecraft is installed as a physical object on the parallel robot platform. The principle of reproduction motion of parallel robot is as follows: input the displacement and rotation parameters of control point P, calculate the length of six legs by position inverse solution, and position closed-loop control of each leg is used to reproduce the position and rotation angle. The relative angle between the spacecraft and the end-effector $\boldsymbol{\Phi}_{ce}$ can be directly used as the angle input of the parallel robot, however, the relative displacement $\boldsymbol{S}_{ce}$ needs to be transformed into the motion parameter of the control point P. The inertial coordinate system of the HIL simulation system is $O_HX_HY_HZ_H$ (the axis directions of which are the same as those of the $O_eX_eY_eZ_e$). The input parameters of control point P are parameters in $O_HX_HY_HZ_H$; in the docking process, the vectors in Fig. 5 satisfy the following relation:

$$\boldsymbol{O_cO_e} = \boldsymbol{S}_{ce} = \boldsymbol{PO}_H - \boldsymbol{O_eO}_H - \boldsymbol{R}_{ce} \cdot \boldsymbol{PO}_c \tag{18}$$

where $\boldsymbol{O_HP}$ indicates the position of control point P in $O_HX_HY_HZ_H$; $\boldsymbol{O_eO_H}$ is the position of end-effector's

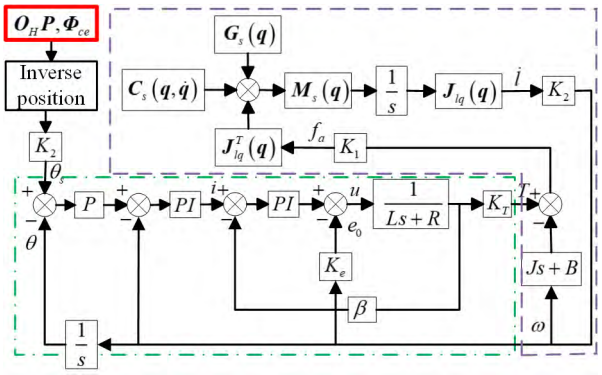

FIGURE 6. A multi-rigid-body dynamics model and a control model of the parallel robot.

centroid in $O_H X_H Y_H Z_H$; $\boldsymbol{PO}_c$ is the position of control point P in$O_c X_c Y_c Z_c$. $\boldsymbol{O_e O_H}$ and $\boldsymbol{PO}_c$ are the known vectors. The transformation matrix $\boldsymbol{R}_{ce}$ can be obtained from the rotation angle $\boldsymbol{\Phi}_{ce}$. Then the displacement vector input to the control point P is:

$$\boldsymbol{PO}_H = \boldsymbol{S}_{ce} + \boldsymbol{O_e O_H} + \boldsymbol{R}_{ce} \cdot \boldsymbol{PO}_c \tag{19}$$

A multi-rigid-body dynamics model and a control model of the parallel robot are shown in Fig. 6. The dotted line region is a multi-rigid-body dynamics model of the parallel robot based on the Kane's method; where q is the six DOF attitude of the parallel robot; $M_s(q)$ denotes the mass matrix of the parallel robot's platform and leg in $O_H X_H Y_H Z_H$; $C_s(q, \dot{q})$ is the Coriolis term in the inertial system; $G_s(q)$ is the gravity and the external force in $O_H X_H Y_H Z_H$; $J_{lq}(q)$ is the velocity Jacobian matrix. The dash-dot line region is the control system model of the control system (consists of driver and motor); where PI denotes the proportional-integral controller; P denotes the proportional controller; L and R are the inductance and resistance of the motor, respectively; K_e is the back EMF coefficient of the motor; K_T is the torque coefficient; J and B are the equivalent inertia and damping of electric cylinder and motor, respectively; K_2 is the velocity conversion coefficient of the electric cylinder and the motor; K_1 is the reciprocal of K_2; β is a current feedback coefficient; f_a and $\dot{l}$ are the output force and line velocity of electric cylinders. The six sets of control systems of the parallel robot have the same characteristics; thus the diagram of the control principle for one set of control system is shown in Fig. 6.

C. CONTACT FORCE AND MOMENT MODEL

The force $\boldsymbol{F}_{mea}$ and moment $\boldsymbol{M}_{mea}$ measured by the force sensor are the values in $O_e X_e Y_e Z_e$; the relationship between $\boldsymbol{F}_{mea}$ ($\boldsymbol{M}_{mea}$) and $\boldsymbol{F}_1$ ($\boldsymbol{M}_1$) is:

$$\begin{cases} \boldsymbol{F}_1 = \boldsymbol{R}_{eg} \cdot \boldsymbol{F}_{mea} \\ \boldsymbol{M}_1 = \boldsymbol{M}_{mea} \end{cases} \tag{20}$$

Take the single point contact of end-effector and target-adapter as an example to calculate $\boldsymbol{F}_2$ and $\boldsymbol{M}_2$ in spacecraft dynamics. C is the contact point in Fig. 5; $\boldsymbol{CO}_e$ and $\boldsymbol{CO}_c$ indicate the vectors of contact point to the end-effector's centroid and to spacecraft's centroid, respectively. The calculation results are shown in formula (21). When the contact is multi-point contact, formula 26 is still applicable.

$$\begin{cases} \boldsymbol{F}_2 = -\boldsymbol{R}_{eg} \cdot \boldsymbol{F}_{mea} \\ \boldsymbol{M}_2 = \boldsymbol{R}_{ce}^{-1} \cdot (\boldsymbol{CO}_c \times (-\boldsymbol{F}_{mea})) \\ \quad = \boldsymbol{R}_{ce}^{-1} \cdot (\boldsymbol{C}_c\boldsymbol{O}_e \times \boldsymbol{F}_{mea} - \boldsymbol{CO}_e \times \boldsymbol{F}_{mea}) \\ \quad = \boldsymbol{R}_{ce}^{-1} \cdot (\boldsymbol{S}_{ce} \times \boldsymbol{F}_{mea} - \boldsymbol{M}_{mea}) \end{cases} \tag{21}$$

In the HIL simulation, the force and moment are affected by the delay of the parallel robot. In order to compensate the force and moment, it is necessary to study the contact characteristics and the mechanism of the DM. The DM inside the end-effector captures and locks the capture-rod through three flexible wire ropes, and then drags the spacecraft. A top view of the state of the three wire ropes and the capture-rod is shown in Fig. 7-a, the two ends of the three wire ropes AA', BB' and CC' are fixed to the moving ring and the stationary ring, respectively. When capturing, the stationary ring remains stationary and the moving ring rotates, causing that the three wire ropes tighten the capture-rod and restrain its horizontal direction. The front view of the wire ropes and the capture-rod is shown in Fig. 7-b. The head of the capture-rod has a hemispherical structure with a groove below it; three wire ropes are tightened at the groove to restrict the capture-rod's vertical direction. Under the constraint of three directions, the drag mechanism drives the moving ring and the stationary ring to move upward (the axial direction of the end-effector) to perform drag operation and so on.

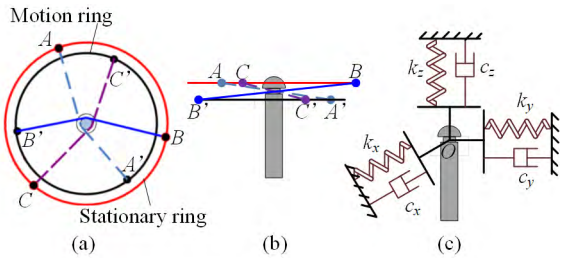

FIGURE 7. Schematic diagram of the contact between the wire rope and the capture rob.

In the docking experiment, if the HIL simulation system does not diverge, the displacements of the point O (the center of the capture-rod groove) relative to its equilibrium position (the resultant force of the capture-rod is zero at this position, which can be measured by the sensor, and set as point O_D) in the radial and axial directions are usually no more than 10 mm under the action of the flexible wire ropes; because the three wire ropes are tightly tied to the capture-rod, the three wire ropes can always maintain contact with the capture-rod within this displacement range. Meanwhile, making that the parallel robot drives the target-adapter along the three axes of the $O_H X_H Y_H Z_H$ (non-dynamics process, the motion range is in the point O motion space), the test results show that the motion along one direction has little effect on the

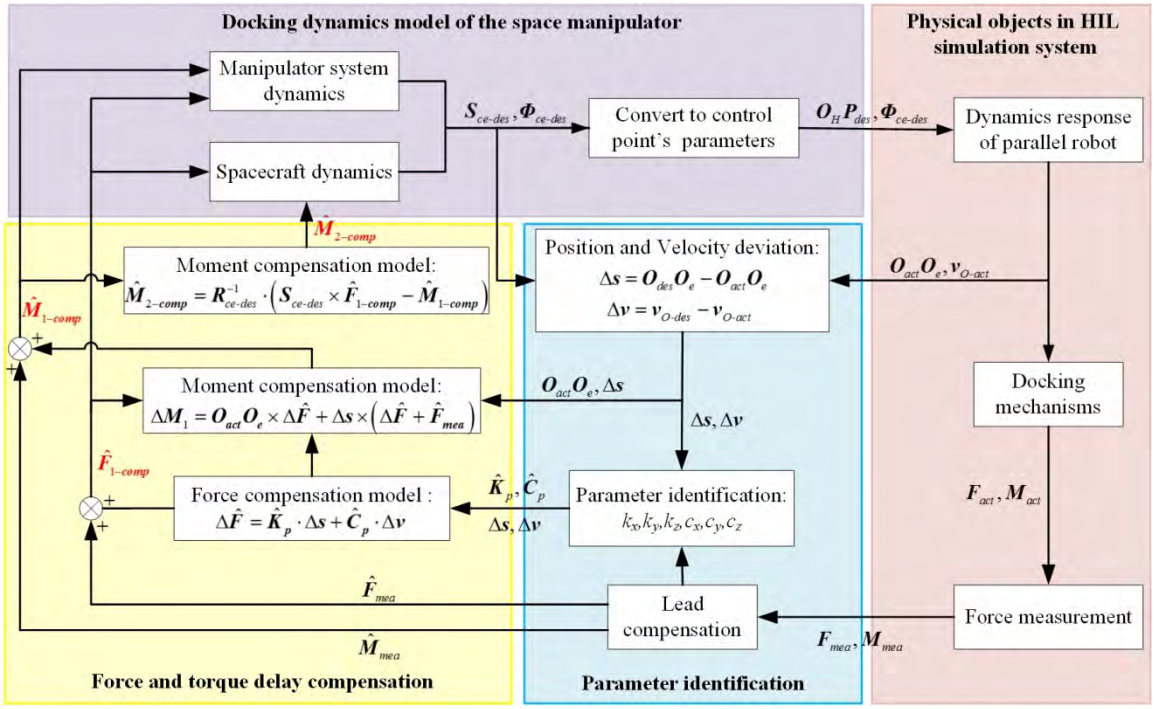

FIGURE 8. Force and moment compensation schematic diagram for space manipulator docking HIL simulation system.

force in the other two directions. Based on the above two premises, the restraint and action of the wire ropes on the capture-rod can be approximated as the restraint and action of three mutually perpendicular stiffness-damping systems on the capture-rod, as shown in Fig. 7-c. The motion of the capture-rod's groove makes the wire rope produce flexible deformation and then produce elastic force. The diameter of the rob at the groove is very fine, usually several millimeters; it is considered that the displacement of point O relative to O_D is the deformation of the stiffness-damping system. Thus, the contact force within radial and axial small displacement range of the point O relative to O_D can be expressed as:

$$\begin{cases} \begin{bmatrix} \boldsymbol{v}_p \\ \boldsymbol{\omega}_p \end{bmatrix} = \boldsymbol{J}_{lq}^{-1} \cdot \dot{\boldsymbol{L}} \\ \boldsymbol{v}_O = \boldsymbol{v}_p + \boldsymbol{\omega}_p \times (\boldsymbol{R}_{ce} \cdot \boldsymbol{OP}) \\ \boldsymbol{v}_{OD} = \boldsymbol{v}_O - \boldsymbol{v}_D \\ \boldsymbol{l}_{OD} = \int_0^t \boldsymbol{v}_{OD} dt \\ \boldsymbol{F}_{mea} = \int_0^t \boldsymbol{K}_p \cdot \boldsymbol{v}_{OD} dt + \boldsymbol{C}_p \cdot \boldsymbol{v}_{OD} \\ \boldsymbol{M}_{mea} = \boldsymbol{OO}_e \times \boldsymbol{F}_1 = (\boldsymbol{S}_{ce} + \boldsymbol{R}_{ce} \cdot (\boldsymbol{PO}_c + \boldsymbol{OP})) \times \boldsymbol{F}_{mea} \end{cases} \tag{22}$$

where $\boldsymbol{v}_O$ indicates the velocity of point O in $O_H X_H Y_H Z_H$; OP is the vector of point O to control point P in the spacecraft body coordinate; $\boldsymbol{J}_{lq}^{-1}$ is the transformation matrix from the velocity of the parallel robot's six legs to velocity of the control point, $\boldsymbol{K}_p$ is a stiffness diagonal matrix consisting of k_x, k_y and k_z; $\boldsymbol{C}_p$ is a damping diagonal matrix consisting of c_x, c_y and c_z; both $\boldsymbol{K}_p$ and $\boldsymbol{C}_p$ are time-varying matrices; $\dot{L}$ is velocity matrix for six legs of parallel robot; $\boldsymbol{v}_D$ is the velocity of the drag mechanism in the end-effector (i.e. the velocity of point O_D); $\boldsymbol{v}_p$ is the velocity of control point P in $O_H X_H Y_H Z_H$; ω_p is the angular velocity of the parallel robot's body coordinate system relative to the $O_H X_H Y_H Z_H$.

When the contact stiffness and damping matrices are known, the force and moment compensation model can be further deduced by the formula (22).

IV. FORCE AND MOMENT COMPENSATION MODEL OF THE HIL SIMULATION FOR MANIPULATOR DOCKING

The force and moment compensation method principle diagram based on the three DOF stiffness-damping on-line identification is shown in Fig. 8. Based on Fig. 4, parameter identification module and force/moment delay compensation module are added. Measurement delay model of the sensor usually can approximate to a first-order model with a delay time of T_f, and then in this study we use a first-order phase lead model to compensate the sensor measurement dynamically. The force and moment delay caused by the parallel robot's dynamic response are mainly studied in the following. If the compensated force $\hat{\boldsymbol{F}}_{1\text{-}comp}$, compensated moment $\hat{\boldsymbol{M}}_{1\text{-}comp}$ and $\hat{\boldsymbol{M}}_{2\text{-}comp}$ are the same as the contact force and moment corresponding to the desired position calculated by the docking dynamics, then the force/moment for dynamics calculation and the dynamics calculation results will not be affected by the dynamic response of the parallel robot; so that the desired position of the dynamics calculation is the same

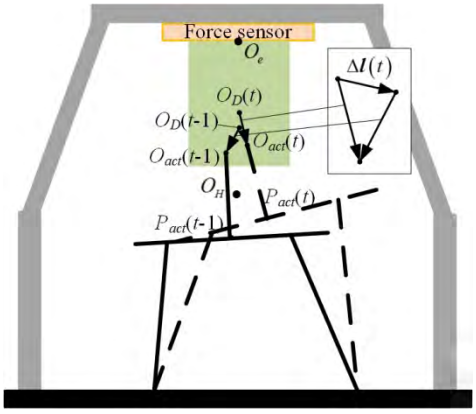

FIGURE 9. Position change of parallel robot in two adjacent sampling periods.

as that of real space docking to prevent the HIL simulation system from diverging.

A. THREE DOF STIFFNESS-DAMPING PARAMETER REAL-TIME IDENTIFICATION BASED ON KALMAN-FILTER

The identification results will be affected by the noise interference of the force sensor and the accidental friction of the mechanisms during the docking process. Thus, Kalman-filter identification method is used for its strong anti-noise interference and good stability; in addition, this identification method has high accuracy for the system with large variation in parameters. In this study, the stiffness and damping parameters are identified by using the relationship between the measurement force change $\boldsymbol{F}(t)$, the displacement variation $\boldsymbol{l}_{OD}(t)$ and the velocity variation $\boldsymbol{v}_{OD}(t)$ of two adjacent sampling times. The positions of the parallel robot at the t time and the t-1 time are shown in Fig. 9. $O_D(t\text{-}1)$, $O_{act}(t-1)$, $P_{act}(t-1)$, $O_D(t)$, $O_{act}(t)$, $P_{act}(t)$ are the actual positions of the point O_D, point O and control point P at t-1 time and t time in the $O_H X_H Y_H Z_H$, respectively. It is assumed that stiffness and damping parameters remain unchanged within two adjacent sampling times. Then the physical quantities at the t time can be obtained from formula (22), as shown in formula (23).

$$\begin{cases} \begin{bmatrix} \boldsymbol{v}_{p\text{-}act}(t) \\ \boldsymbol{\omega}_{p\text{-}act}(t) \end{bmatrix} = \boldsymbol{J}_{lq}^{-1}(t) \cdot \dot{\boldsymbol{L}}(t) \\ \boldsymbol{v}_{O\text{-}act}(t) = \boldsymbol{v}_{p\text{-}act}(t) + \boldsymbol{\omega}_{p\text{-}act}(t) \times (\boldsymbol{R}_{ce\text{-}act}(t) \cdot \boldsymbol{OP}) \\ \boldsymbol{v}_{OD}(t) = \boldsymbol{v}_{O\text{-}act}(t) - \boldsymbol{v}_D(t) \\ \Delta\boldsymbol{v}_{OD}(t) = \boldsymbol{v}_{OD}(t) - \boldsymbol{v}_{OD}(t-1) \\ \Delta\boldsymbol{l}_{OD}(t) = \int_0^t \boldsymbol{v}_{OD}(t)\,dt - \int_0^{t-1} \boldsymbol{v}_{OD}(t)\,dt \\ \Delta\boldsymbol{F}_{mea}(t) = \boldsymbol{K}_p(t) \cdot \Delta\boldsymbol{l}_{OD}(t) + \boldsymbol{C}_p(t) \cdot \Delta\boldsymbol{v}_{OD}(t) \end{cases} \tag{23}$$

The velocity and displacement of six legs can be measured in real time, then $\boldsymbol{l}_{OD}(t)$ and $\boldsymbol{v}_{OD}(t)$ can be calculated according to the formula (23); meanwhile, $\hat{F}_{mea}(t)$ can be calculated by the measurement values of the sensor; then the identification of stiffness and damping parameters in three directions is carried out by combining the formula 23-6 and Kalman-filter identification method. Taking the X axis as an example, the identification process of k_x and c_x is explained. We assume that the linear system of formula 23-6 can be described as:

$$\begin{cases} Y(k+1) = \Phi(k+1,k)\,Y(k+1) + \Gamma(k+1,k)\,W(k) \\ Z(k) = H(k)\,Y(k) + V(k) \end{cases} \tag{24}$$

where $W(k)$ is the friction noise and sensor measurement noise, $V(k)$ is the system process noise.

$$\begin{cases} \Gamma = \Phi = I \\ Z(k) = \Delta\hat{F}_{mea\text{-}x}(k) \\ H(k) = \begin{bmatrix} \Delta l_{OD\text{-}x}(k) & \Delta v_{OD\text{-}x}(k) \end{bmatrix} \\ Y(k) = \begin{bmatrix} k_x(k) & c_x(k) \end{bmatrix}^T \end{cases} \tag{25}$$

where $\hat{F}_{mea\text{-}x}(k)$, $l_{OD\text{-}x}(k)$ and $v_{OD\text{-}x}(k)$ are the measurement force variation, displacement variation and velocity variation in the X direction, respectively.

The Kalman-filter identification model is as follows:

$$\begin{cases} \hat{Y}(k|k) = \hat{Y}(k-1|k-1) \\ \qquad\qquad + K(k)\left[Z(k) - H(k)\,\hat{Y}(k-1|k-1)\right] \\ K(k) = \dfrac{P(k|k-1)\,H^T(k)}{\left[H(k)\,P(k|k-1)\,H^T(k) + R_k\right]} \\ P(k|k-1) = P(k|k-1) + Q_{k-1} \\ P(k|k) = [I - K(k)\,H(k)]\,P(k|k-1) \end{cases} \tag{26}$$

where Q_{k-1} and R_k are the covariance matrixes of $V(k)$ and $W(k)$, respectively; $P(k|k)$ is the error covariance matrix; $K(k)$ is the Kalman-gain; $Y(k|k) = [k_x(k) c_x(k)]$.

The initial values of Y(0|0) and P(0|0) need to be set before the identification. The stiffness and damping identification processes in the Y axis and the Z axis are as same as those mentioned above.

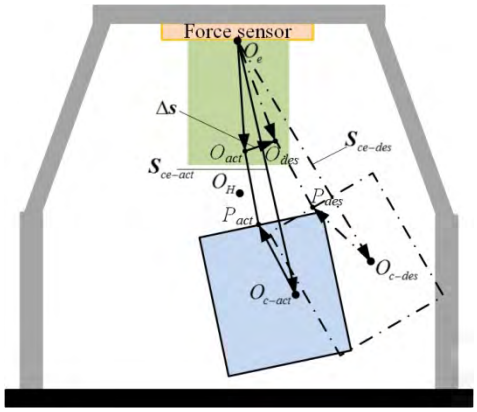

FIGURE 10. The schematic diagram the desired position and the actual position.

B. CONTACT FORCE AND MOMENT DELAY COMPENSATION

The contact stiffness and damping matrices $\hat{\boldsymbol{K}}_p$ and $\hat{\boldsymbol{C}}_p$ at t time are obtained by identification; the contact force and

moment compensation model at t time is deduced from the deviation between the desired position and the actual position of the parallel robot. The schematic diagram the desired position and the actual position at t time is shown in Fig. 10. The 'act' and 'des' marks in the lower corner of the variable name represent the actual position and the desired position of the point or vector, respectively. For the sake of simplicity, the state of the parallel robot in two positions is not depicted in Fig. 10. The solid line and the dotted line represent the actual position and the desired position of the virtual spacecraft, respectively. The position deviation between the actual position and the desired position of point O is $\boldsymbol{s}$.

The desired velocity of point O can be calculated by the docking dynamics:

$$\boldsymbol{v}_{O\text{-}des} = \boldsymbol{V}_{ce} + (\boldsymbol{R}_{ce\text{-}des} \cdot \omega_c) \times (\boldsymbol{R}_{ce\text{-}des} \cdot (\boldsymbol{PO}_c + \boldsymbol{OP})) \tag{27}$$

The actual velocity of point O can be calculated by formula 23-1 and 23-2, and then the velocity deviation between actual position and desired position is:

$$\Delta \boldsymbol{v} = \boldsymbol{v}_{O\text{-}des} - \left(\boldsymbol{v}_{p\text{-}act} + \boldsymbol{\omega}_{p\text{-}act} \times (\boldsymbol{R}_{ce\text{-}act} \cdot \boldsymbol{OP})\right) \tag{28}$$

Position deviation of point O between actual position and desired position is:

$$\Delta \boldsymbol{s} = \boldsymbol{P}_{des}\boldsymbol{O}_H + \boldsymbol{R}_{ce\text{-}des} \cdot \boldsymbol{OP} - (\boldsymbol{P}_{act}\boldsymbol{O}_H + \boldsymbol{R}_{ce\text{-}act} \cdot \boldsymbol{OP}) \tag{29}$$

Then the contact force compensation model is:

$$\Delta \hat{\boldsymbol{F}} = \hat{\boldsymbol{K}}_p \cdot \Delta \boldsymbol{s} + \hat{\boldsymbol{C}}_p \cdot \Delta \boldsymbol{v} \tag{30}$$

Then the compensated force is:

$$\hat{\boldsymbol{F}}_{1\text{-}comp} = \hat{\boldsymbol{F}}_{mea} + \Delta \hat{\boldsymbol{F}} \tag{31}$$

The moment generated by the contact force at the desired position is regard as:

$$\begin{aligned} \boldsymbol{M} &= (\boldsymbol{O}_{act}\boldsymbol{O}_e + \Delta s) \times \left(\hat{\boldsymbol{F}}_{mea} + \Delta \hat{\boldsymbol{F}}\right) \\ &= \boldsymbol{O}_{act}\boldsymbol{O}_e \times \boldsymbol{F}_{mea} + \boldsymbol{O}_{act}\boldsymbol{O}_e \times \Delta \hat{\boldsymbol{F}} \\ &\quad + \Delta \boldsymbol{s} \times \hat{\boldsymbol{F}}_{mea} + \Delta \boldsymbol{s} \times \Delta \hat{\boldsymbol{F}} \end{aligned} \tag{32}$$

$\boldsymbol{O}_{act}\boldsymbol{O}_e \times \boldsymbol{F}_{mea}$ is considered as the moment $\hat{\boldsymbol{M}}_{mea}$ measured by sensor, then the moment compensation model is:

$$\begin{aligned} \Delta \boldsymbol{M} &= O_{act}\boldsymbol{O}_e \times \Delta \hat{\boldsymbol{F}} + \Delta \boldsymbol{s} \times \hat{\boldsymbol{F}}_{mea} + \Delta \boldsymbol{s} \times \Delta \hat{\boldsymbol{F}} \\ &= (\boldsymbol{S}_{ce\text{-}act} + \boldsymbol{R}_{ce\text{-}act} \cdot (\boldsymbol{PO}_c + \boldsymbol{OP})) \\ &\quad \times \Delta \hat{\boldsymbol{F}} + \Delta \boldsymbol{s} \times \hat{\boldsymbol{F}}_{mea} + \Delta \boldsymbol{s} \times \Delta \hat{\boldsymbol{F}} \end{aligned} \tag{33}$$

The compensated moment is:

$$\hat{\boldsymbol{M}}_{1\text{-}comp} = \hat{\boldsymbol{M}}_{mea} + \Delta \boldsymbol{M} \tag{34}$$

The compensated contact force and moment input to the manipulator system can be obtained by formula 25:

$$\begin{cases} \boldsymbol{F}_1 = \boldsymbol{R}_{eg} \cdot \hat{\boldsymbol{F}}_{1\text{-}comp} \\ \boldsymbol{M}_1 = \hat{\boldsymbol{M}}_{1\text{-}comp} \end{cases} \tag{35}$$

The compensated contact force and moment input to the spacecraft can be obtained by formula 26:

$$\begin{cases} \boldsymbol{F}_2 = -\boldsymbol{R}_{eg} \cdot \hat{\boldsymbol{F}}_{1\text{-}comp} \\ \boldsymbol{M}_2 = \boldsymbol{R}_{ce\text{-}des}^{-1} \cdot \left(\boldsymbol{S}_{ce\text{-}des} \times \hat{\boldsymbol{F}}_{1\text{-}comp} - \hat{\boldsymbol{M}}_{1\text{-}comp}\right) \end{cases} \tag{36}$$

V. VERIFICATIONS

A. SIMULATION VERIFICATIONS

The HIL simulation system model for space manipulator, as shown in Fig. 8, was established using the Simulink module of the Matlab software. The drag mechanism moves at a constant velocity, thus, the displacement curve of the parallel robot is close to an oblique line. However, it is difficult to observe the frequency characteristics and the reproduction accuracy under the gradual curves. The oscillation curves are convenient to compare the performances of different compensation methods. So set that the drag mechanism was stationary in the simulation and experiment, respectively. And the parallel robot offset downward a certain displacement from the equilibrium position, respectively, which made the wire rope deform. Then the HIL simulation system came into the dynamics stage to simulate the motion of the spacecraft under the action of flexible wire rope. The force and moment delay compensation (FAMDC) results, uncompensated results and ideal results are compared to verify the effectiveness of the compensation method proposed in this paper.

TABLE 1. Docking parameters of single-DOF.

Parameters	Value
Mass of spacecraft m_c (kg)	2000
Mass of end-effector m_e (kg)	300
Mass of space station m_s (kg)	50000
Stiffness of manipulator k'_z (N/m)	1.5e5
Damping of manipulator c'_z (N/(m/s))	200
Contact stiffness k_z (N/m)	5e4
Contact damping c_z (N/(m/s))	100

1) VERIFICATION OF SINGLE-DOF DOCKING

Assuming that the manipulator docking only produces motion in one direction (Z direction), the effectiveness of the compensation method in simple cases will be verified. The simulation parameters are shown in Table 1. The parallel robot offsets 10 mm from the equilibrium position along Z direction, and then the HIL simulation system comes into the dynamics stage. The motion of the control point with different compensation conditions are shown in Fig. 11. The 'FAMDC-dc' and 'FAMDC-pr' are the dynamics calculation motion and actual motion after using the FAMDC method, respectively; 'Without compensation' is the actual motion without using compensation method; 'Ideal' refers to the motion of the parallel robot without delay (real space docking condition). We can get that the motion of the control point is divergent without the compensation method; after using

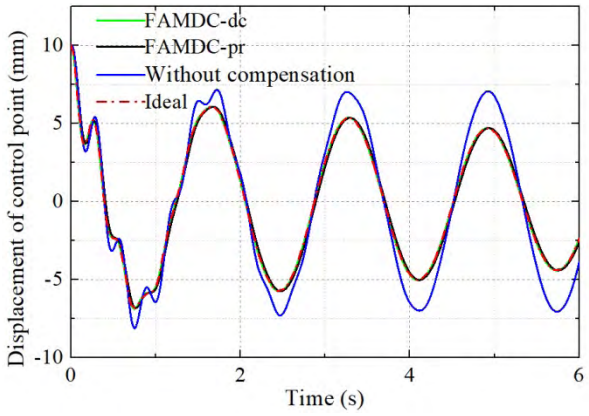

FIGURE 11. Motion of the control point under different compensation conditions.

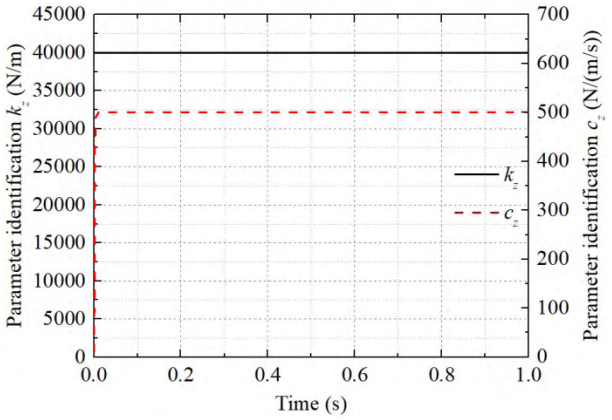

FIGURE 12. Identification results of the k_z and c_z.

the FAMDC method, the motion obtained by the dynamics calculation is basically the same as that of the ideal motion, which indicates that the proposed FAMDC method can prevent the divergence of the system. Due to the displacement phase delay of the parallel robot, the actual motion has little amplitude and phase deviation relative to the motion calculated by dynamics.

Set the initial values Y(0|0)=[10 10]. The identification results of contact stiffness and damping with noise are shown in Fig. 12, which indicate the Kalman-filter identification method can quickly obtain accurate results in the case of noise.

The ideal force, the contact force without compensation and the compensated force with FAMDC method are given in Fig. 13. It shows that the contact force without compensation is divergent, while the value of the compensated force is close to the ideal one. The results indicate that the FAMDC method eliminates the amplitude and phase deviation of the force caused by the parallel robot's response delay, so that the compensated force, the desired force corresponding to the desired position and the ideal force are the same. Then, the motion of the dynamics calculation is consistent with the ideal motion; the system is no longer divergent.

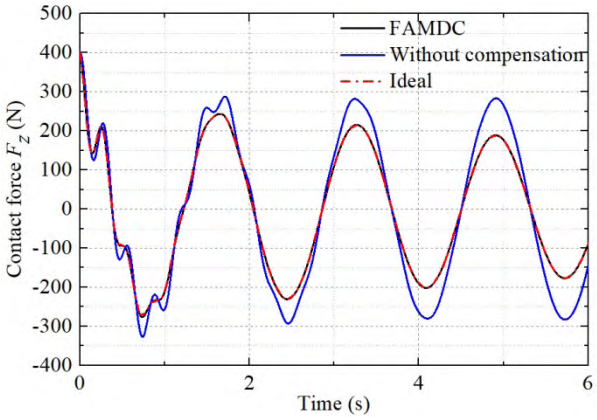

FIGURE 13. Contact forces under different compensation conditions.

TABLE 2. Docking parameters of multi-DOF.

Parameters	Value
Mass of spacecraft m_c (kg)	2000
Mass of end-effector m_e (kg)	300
Mass of space station m_s (kg)	50000
Inertia of spacecraft I_{xx}, I_{yy}, I_{zz} (kg·m^2)	2e3,2e3,2e3
Inertia of end-effector I_{xx}, I_{yy}, I_{zz} (kg·m^2)	300,300,300
Inertia of space station I_{xx}, I_{yy}, I_{zz} (kg·m^2)	6e4,6e4,6e4
Stiffness of manipulator k'_{xx}, k'_{yy}, k'_{zz} (N/m)	1e4,1e4,1e4
Damping of manipulator c'_{xx}, c'_{yy}, c'_{zz} (N/(m/s))	400, 400, 400
Contact stiffness k_{xx}, k_{yy}, k_{zz} (N/m)	4e4,3.6e4,3.2e4
Contact damping c_{xx}, c_{yy}, c_{zz} (N/(m/s))	400,240,320

2) VERIFICATION OF SIX DOF DOCKING

The simulation parameters are shown in Table 2. The parallel robot offsets 10 mm from the equilibrium position along X, Y and Z directions, respectively, then the HIL simulation system comes into the dynamics stage to compare of control point's motion parameters [$\boldsymbol{PO}_{\mathbf{H}}$ $\boldsymbol{\Phi}_{\mathrm{ce}}$] under different compensation conditions. Due to the large number of six DOF motion curves, the 'FAMDC-dc' curves are no longer drawn. The validity of the FAMDC method to prevent the system divergence is evaluated by the actual motion curves and the ideal curves, which are shown in Fig. 14. 'Without compensation' curves are drawn separately, as shown in Fig. 15. From the displacement curves in Fig. 14, it can be seen that: the docking system has two oscillation frequencies; the high-frequency oscillation attenuates quickly under the action of damping; and the low-frequency oscillation is mainly reflected in the later period. The FAMDC method can not only ensure the stability of high-frequency oscillation, but also ensure high reproduction accuracy. The curves in Fig. 15 diverge at high-frequency, which shows that the FAMDC method effectively solves the problems of system stability and reproduction accuracy in the process of six DOF docking.

Set the stiffness and damping initial values in three directions are Y(0|0)=[10 10]. The contact stiffness and

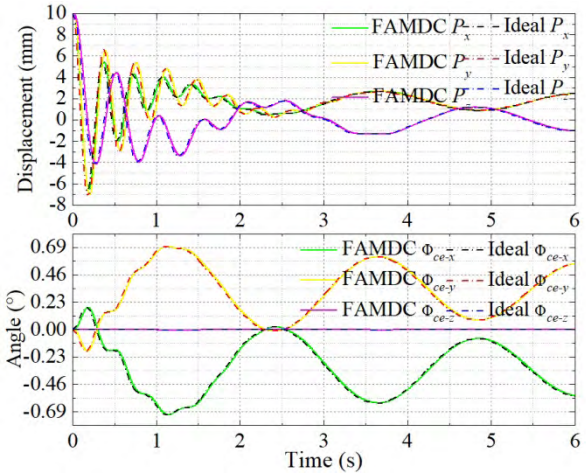

FIGURE 14. Motion of the control point under different compensation conditions.

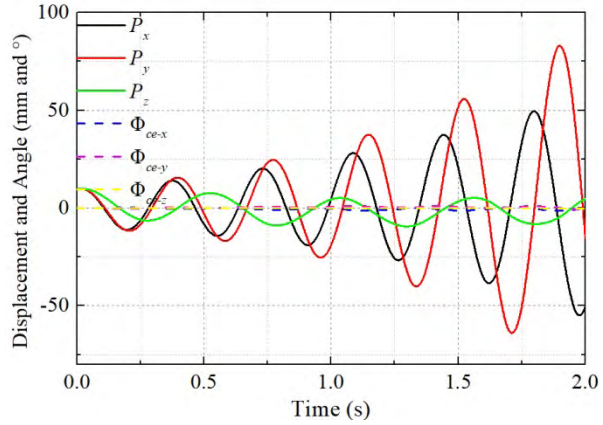

FIGURE 15. Motion of the control point without compensation.

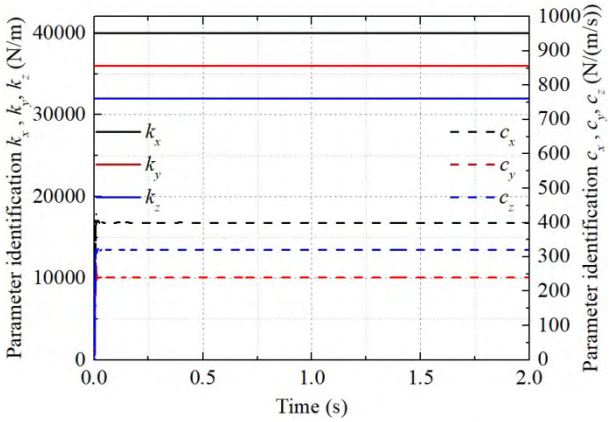

FIGURE 16. Identification results of the k_x, k_y, k_z, c_x, c_y and c_z.

damping verification results with noise interference are shown in Fig. 16, which reach the accuracy values from the initial values in several milliseconds.

In the case of no compensation, the force and moment curves are divergent. The ideal force and moment and the compensated force and moment with FAMDC method are

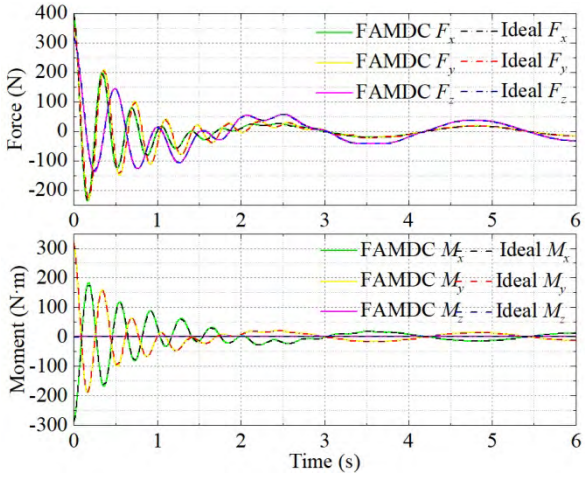

FIGURE 17. Force and moment compensation results.

given in Fig. 17. The values of the compensated force and moment are close to the ideal ones, which show that the compensated force and moment are the same as the desired force and moment corresponding to the desired position of dynamics calculation. The HIL simulation system has high reproduction accuracy.

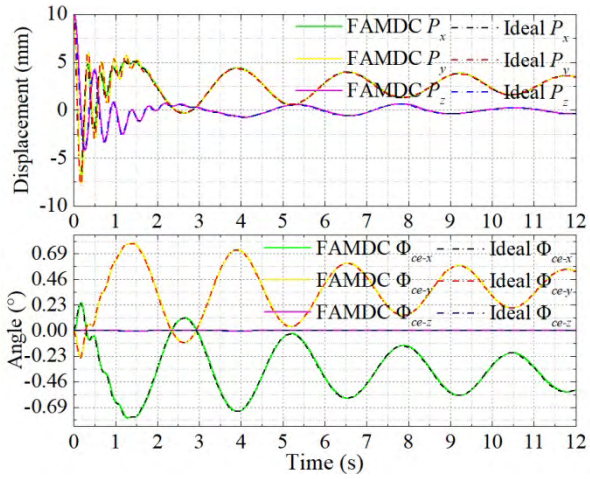

FIGURE 18. Motion of the control point under different compensation conditions.

3) VERIFICATION OF SIX DOF DOCKING WITH TIME-VARYING CONTACT PARAMETERS

On the basis of the simulation parameters in Table 2, triangular wave signals with amplitudes of 4e4N/m, 3.6e4N/m and 3.2e4N/m and periods of 4 s are superposed with the contact stiffness k_x, k_y and k_z, respectively, triangular wave signals with amplitudes of 400N/(m/s), 240N/(m/s) and 320N/(m/s) and periods of 4 s are superposed with the contact stiffness c_x, c_y and c_z, respectively; which are used to simulate the time-varying docking parameters. The increase of the contact stiffness will still make the uncompensated system diverge. The actual motion curves and ideal curves are shown in Fig. 18. The results show that the FAMDC method can still

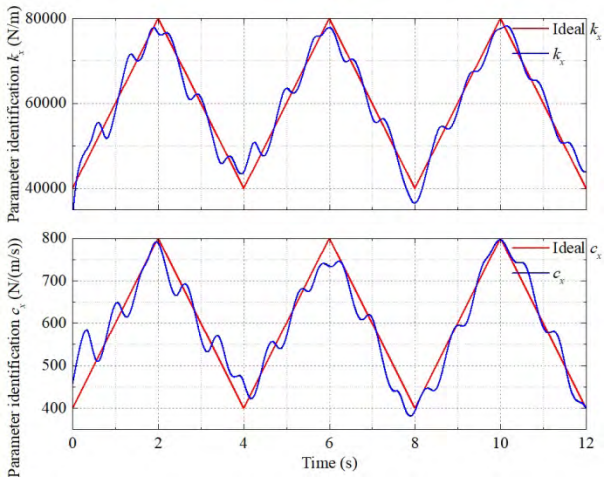

FIGURE 19. Identification results of the k_X and c_X.

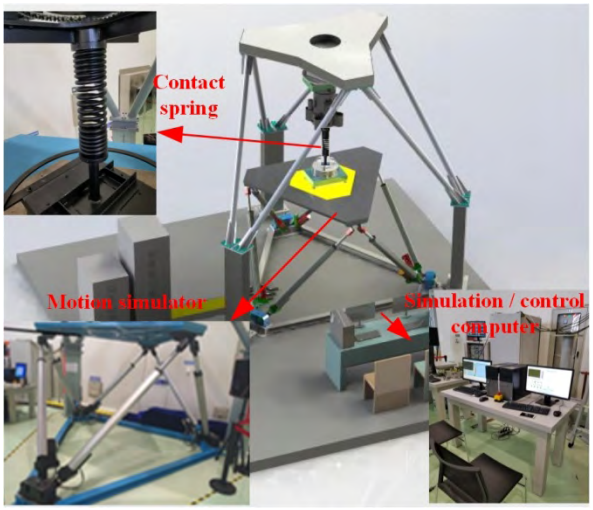

FIGURE 20. The experimental facilities of the HIL simulation system.

prevent the divergence of the system and ensure high reproduction accuracy when the contact parameters vary in a wide range.

Identification results of contact stiffness and damping with noise interference are shown in Fig. 19. The identification results of stiffness and damping in X direction are taken as an example to illustrate the accuracy of Kalman-filter identification method in identifying time-varying parameters. We can get that the identification results of stiffness and damping can accurately follow the variable stiffness and damping.

The simulation results show that the force and moment compensation method based on three DOF stiffness-damping identification can effectively solve the instability problem caused by the dynamic response delay of the parallel robot in the HIL simulation system. In addition, the proposed compensation method can ensure high reproduction accuracy.

B. EXPERIMENTAL VERIFICATIONS

The experimental facilities of the HIL simulation system for manipulator docking were shown in Fig. 20. Due to the classified reasons, pictures of the end-effector and the target-adapter can't be provided, and pictures of the other main structures were presented separately. Because that the contact stiffness in the three directions are unknown, it is not easy to explain the accuracy of the identification results and the compensation results; therefore, a spring with known stiffness and damping (the stiffness of the spring was within the stiffness range of the wire rope) was used to simulate the elasticity in one direction. The correctness of the identification results and the effectiveness of the compensation method are verified by the single-DOF motion, and then the wire rope is used to capture and fix the capture-rod of the target-adapter to further verify the compensation effect of six DOF force and moment.

1) VERIFICATION OF SINGLE-DOF DOCKING

Generally, the greater the stiffness of the system is, the higher the dynamics frequency is, and then the worse the stability of the HIL simulation system is. Thus experiments are carried out with two sets of parameters to illustrate the effectiveness of the FAMDC method. The main parameters of the lower dynamics frequency experiment are shown in Table 3-I. The high dynamics frequency ω_{high} is 2.13 Hz and the low dynamics frequency ω_{low} is 0.54 Hz.

TABLE 3. Docking parameters of single-DOF.

Parameters	I	II
Mass of spacecraft m_c (kg)	1000	500
Mass of end-effector m_e (kg)	500	200
Mass of space station m_s (kg)	50000	50000
Stiffness of manipulator k'_z (N/m)	20000	1e5
Damping of manipulator c'_z (N/(m/s))	600	600
Stiffness of spring k_z (N/m)	5e4	5e4
Damping of spring c_z (N/(m/s))	120	120

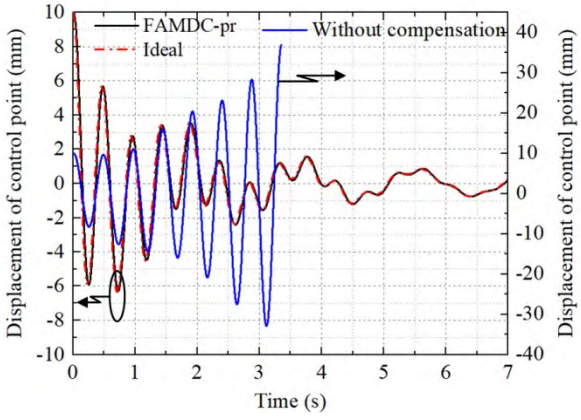

FIGURE 21. Motion of the control point with different compensation conditions.

The parallel robot offsets 10 mm from the equilibrium position along Z direction, then the HIL simulation system comes into the dynamics stage. The motion of the control point with different compensation conditions are shown in Fig. 21.

The motion curve oscillates and diverges at ω_{high} without the compensation method; to prevent excessive contact force, the experiment is stopped at 3.4 s; using the FAMDC compensation method, the actual motion curve basically coincides with the ideal motion curve, which indicates the effectiveness of FAMDC method in preventing system divergence.

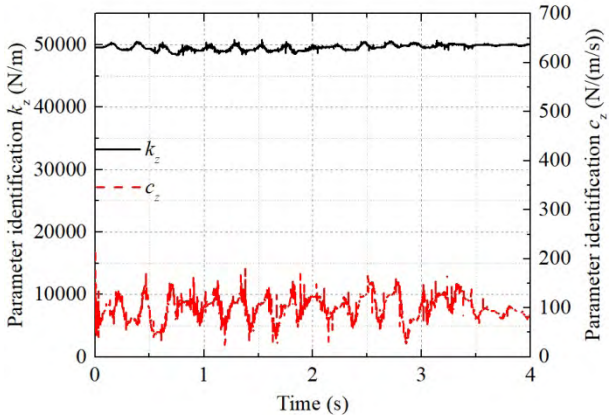

FIGURE 22. Identification results of the k_z and c_z.

Set the initial values Y(0|0)=[10 10]. The identification results of contact stiffness and damping are shown in Fig. 22. Stiffness reaches the accuracy value in several milliseconds. There may be small gaps between the mechanisms or there is other force noise interference; which is the main reason for slightly deviation between the accuracy values and the identification results, and the deviation is within ±2%. The damping value is small, and the force induced by damping is smaller than that induced by stiffness, therefore, the deviation value between identification results and the accuracy value is relatively large, but the average value and the accurate value are basically the same.

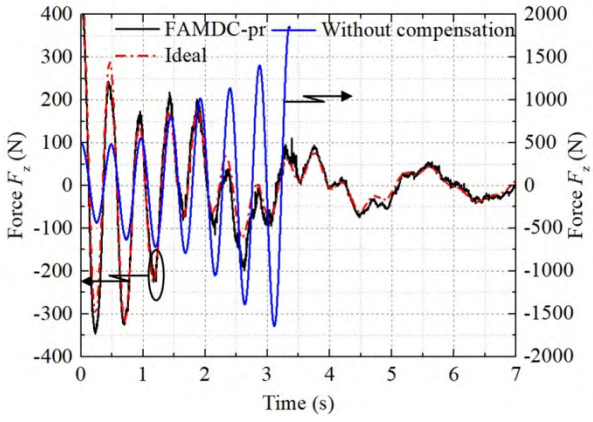

FIGURE 23. Contact forces under different compensation conditions.

The ideal force, the measurement contact force without compensation and the compensated force with FAMDC method are given in Fig. 23. It shows that the measurement force without compensation is divergent, while the value of the compensated force is close to the ideal one. The results indicate that parameter identification results and FAMDC method can make the compensated force basically be equal to the desired force corresponding to the desired position, and further can ensure the high reproduction of the HIL simulation system.

The main parameters of the higher dynamics frequency experiment are shown in Table 3-II. The high dynamics frequency ω_{high} is 4.47 Hz and the low dynamics frequency ω_{low} is 1.28 Hz. The motion of the control point with different compensation conditions are shown in Fig. 24. Without the compensation method, the actual motion curve diverges at ω_{high} and ω_{low}, respectively; after using FAMDC method, the actual motion curve coincides with the ideal curve, which has high simulation precision.

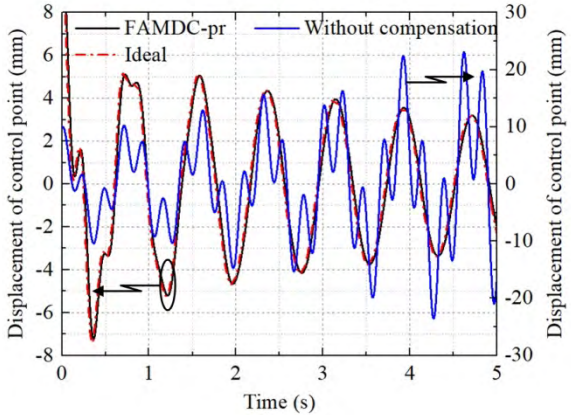

FIGURE 24. Motion of the control point with different compensation conditions.

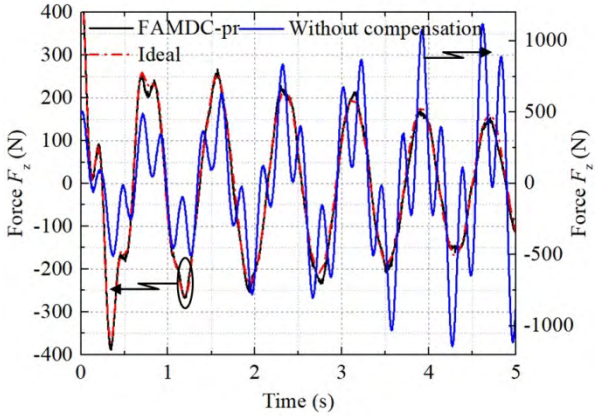

FIGURE 25. Contact forces under different compensation conditions.

The ideal force, the measurement contact force without compensation and the compensated force with FAMDC method are given in Fig. 25. It shows that the measurement force without compensation is divergent, while the value of the compensated force is close to the ideal one. It indicates that the identification results still have good accuracy and the FAMDC method has a good compensation effect in high frequency motion.

2) VERIFICATION OF SIX DOF DOCKING

The experimental parameters are shown in Table 4. The parallel robot offsets 10 mm from the equilibrium position along X, Y and Z directions, then the HIL simulation system comes into the dynamics stage.

TABLE 4. Docking parameters of multi-DOF.

Parameters	Value
Mass of spacecraft m_c (kg)	5000
Mass of end-effector m_e (kg)	300
Mass of space station m_s (kg)	50000
Inertia of spacecraft I_{xx}, I_{yy}, I_{zz} (kg·m^2)	5e3,5e3,5e3
Inertia of end-effector I_{xx}, I_{yy}, I_{zz} (kg·m^2)	500,500,500
Inertia of space station I_{xx}, I_{yy}, I_{zz} (kg·m^2)	6e4,6e4,6e4
Stiffness of manipulator k'_{xx}, k'_{yy}, k'_{zz} (N/m)	8e4,8e4,8e4
Damping of manipulator c'_{xx}, c'_{yy}, c'_{zz} (N/(m/s))	1e3, 1e3, 1e3

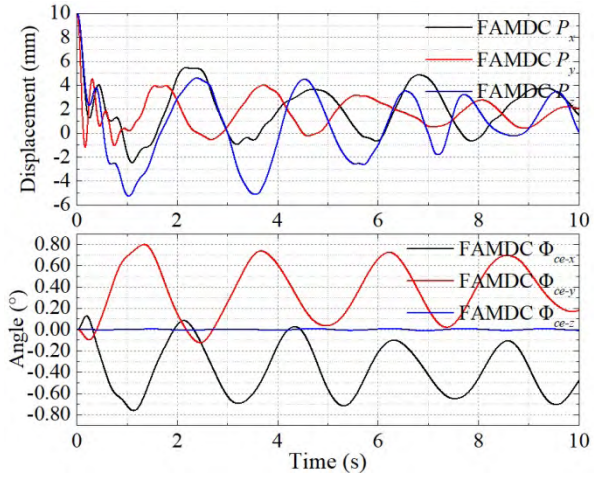

FIGURE 26. Motion of the control point with FAMDC compensation method.

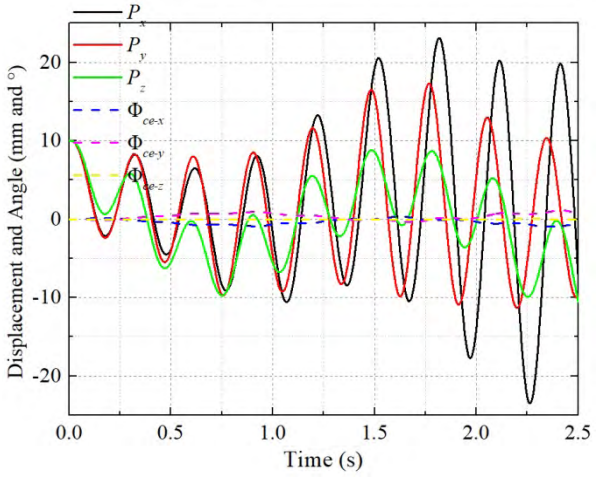

FIGURE 27. Motion of the control point without compensation.

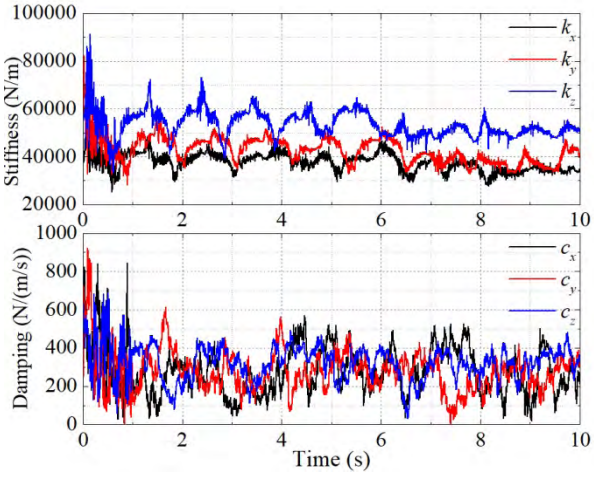

FIGURE 28. The stiffness and damping identification results of three DOF.

The motion curves of the control point with FAMDC method and without compensation are shown in Fig. 26 and Fig. 27, respectively. The motion of the control point without compensation diverges at high frequency; after applying the FAMDC method, the motion of the six DOF converges. The results show that the FAMDC method prevents the system from diverging.

The stiffness and damping identification results of three DOF are shown in Fig. 28. Fig. 26 shows that there is a high frequency motion in 1 s; because the stiffness and damping parameters in different positions will vary, the identification results in Fig. 28 change obviously and quickly in 1 s; with the attenuation of high frequency oscillation, the identification results become relatively stable with the control point's motion after 1 s. Comparing with Fig. 26 and Fig. 28, the stiffness value is maximum when the control point moves to the maximum displacement of positive or negative direction, and the stiffness value is minimum when the control point is near the equilibrium position; which indicates that the stiffness of wire rope increases with the increase of deformation. With the convergence of the control point's displacement, the system oscillation amplitude decreases, and then deformation of the wire rope decreases; which makes the oscillation amplitude of the stiffness decrease. To illustrate the accuracy of the identification results, the parallel robot is made move in three directions, and several positions are selected to calculate the stiffnesses in three directions; the results show that the stiffness ranges obtained by testing in the three directions are basically consistent with the ranges of the identification results, which shows that the identification results are reliable.

The experimental results show that the identification method based on Kalman-filter can accurately obtain the time-varying contact parameters, and the force and moment compensation method based on three DOF stiffness and damping identification can effectively prevent the divergence of the system, and can make the HIL simulation system with high reproduction accuracy.

VI. CONCLUSION

Aiming at the requirements and characteristics of space manipulator docking, a space manipulator docking HIL system is designed in this paper, the docking dynamics model of space manipulator is established. Considering the instability of HIL system caused by the delay of the parallel robot, a method of force and moment compensation based on stiffness and damping identifications in three mutually perpendicular directions is proposed to compensate for the deviation of contact force and moment caused by the delay. Based on the compensation, the compensated force and moment at any time are equal to the desired force and moment corresponding to the desired position in the dynamics calculation; which ensures that the force and moment input to the dynamics calculation are not affected by the delay and prevents the divergence of the system. The simulation and experimental results show that the accuracy of Kalman-filter identification method and the force and moment compensation method based on three DOF stiffness-damping can effectively improve the stability and reproduction accuracy of multi-DOF space docking HIL simulation system.

REFERENCES

[1] K. F. Zhang, H. Zhou, and Q. P. Wen, "Review of the development of robotic manipulator for international space station," *Chin. J. Space Sci.*, vol. 30, no. 6, pp. 612–619, 2010.
[2] W. H. Zhang *et al.*, "Development summarizing of space robot technology national and outside," (in Chinese), *Flight Dyn.*, vol. 31, no. 3, pp. 198–202, 2013.
[3] F. Feng, Y. Liu, H. Liu, and H. Cai, "Design schemes and comparison research of the end-effector of large space manipulator," *Chin. J. Mech. Eng.*, vol. 25, no. 4, pp. 674–687, 2012.
[4] O. Ma and G. Yang, "Validation of a satellite docking simulator using the SOSS experimental testbed," in *Proc. IEEE/RSJ Int. Conf. Intell. Robot. Syst.*, Oct. 2006, pp. 4115–4120.
[5] H. Yang, Z. Xie, K. Sun, X. Zhao, M. Jin, and C. Li, "Development of ground experiment system for space end-effector capturing the floating target in 3-dimensional space," *Ind. Robot.*, vol. 42, no. 4, pp. 347–358, 2015.
[6] H. Yang, M. Jin, Z. Xie, Y. Zhang, K. Sun, and X. Zhao, "Ground microgravity verification of free-floating non-cooperative satellite docking," in *Proc. IEEE Int. Conf. Adv. Intell. Mechatronics (AIM)*, Jul. 2015, pp. 1253–1258.
[7] O. Ma, A. Flores-Abad, and T. Boge, "Use of industrial robots for hardware-in-the-loop simulation of satellite rendezvous and docking," *Acta Astronaut.*, vol. 81, no. 1, pp. 335–347, 2012.
[8] H. Y. Zhao and S. Zhang, "Stability research of space docking dynamics simulation based on stewart platform," *Mach. Tool Hydraul.*, vol. 8, pp. 1–7, Aug. 2006.
[9] F. Feng, "Research on space large misalignment tolerance end-effector and its soft capture strategy," (in Chinese). Ph.D. dissertation, Dept. Mech. Eng., Harbin Inst. Technol., Harbin, China, 2013.
[10] M. Zebenay, T. Boge, R. Krenn, and D. Choukroun, "Analytical and experimental stability investigation of a hardware-in-the-loop satellite docking simulator," *Proc. Inst. Mech. Eng. G, J. Aerosp. Eng.*, vol. 229, no. 4, pp. 666–681, 2015.
[11] H. Zhao and S. Y. Zhang, "Stability analysis of the whole dynamics simulation system of space docking," *J. Wuhan Univ. Sci. Tech. (Natural Sci. Ed.)*, vol. 31, no. 1, pp. 87–90, 2008.
[12] Q. T. Huang, H. Z. Jiang, S. Y. Zhang, and J. W. Han, "Spacecraft docking simulation using hardware-in-the-loop simulator with stewart platform," *Chin. J. Mech. Eng.*, vol. 18, no. 3, pp. 415–418, 2005.
[13] T. Chang, D. Cong, Z. Ye, and J. Han, "Time problems in HIL simulation for on-orbit docking and compensation," in *Proc. 2nd IEEE Conf. Ind. Electron. Appl.*, May 2007, pp. 841–846.
[14] H. Shimoji, M. Inoue, K. Tsuchiya, K. Niomiya, and I. K. J. Nakatani, "Simulation system for a space robot using six-axis servos," *Adv. Robot.*, vol. 6, no. 2, pp. 179–196, 1991.
[15] K. Osaki, A. Konno, and M. Uchiyama, "Delay time compensation for a hybrid simulator," *Adv. Robot.*, vol. 24, nos. 8–9, pp. 1081–1098, 2010.
[16] S. Abiko, Y. Satake, X. Jiang, T. Tsujita, and M. Uchiyama, "Delay time compensation based on coefficient of restitution for collision hybrid motion simulator," *Adv. Robot.*, vol. 28, no. 17, pp. 1177–1188, 2014.
[17] S. Ananthakrishnan, R. Teders, and K. Alder, "Role of estimation in real-time contact dynamics enhancement of space station engineering facility," *IEEE Robot. Autom. Mag.*, vol. 3, no. 3, pp. 20–28, Sep. 1996.
[18] C. Qi, X. Zhao, F. Gao, A. Ren, and Y. Hu, "Divergence compensation for hardware-in-the-loop simulation of stiffness-varying discrete contact in space," *Acta Astronaut.*, vol. 128, pp. 295–303, Nov./Dec. 2016.
[19] S. Yu, J. Han, Z. Qu, and Y. Yang, "A force and displacement compensation method toward divergence and accuracy of hardware-in-the-loop simulation system for manipulator docking," *IEEE Access*, vol. 6, pp. 35091–35104, 2018.

SIMIAO YU was born in Mudanjiang, Heilongjiang, China, in 1988. He received the B.S. degree from the College of Mechanical and Electrical Engineering, Harbin University of Science and Technology, in 2011, and the M.S. degree from the School of Mechanical Design, Harbin Institute of Technology, China, in 2013, where he is currently pursuing the Ph.D. degree. His research interests include electromechanical servo control, system identification, modeling and control of system, modeling and control of the parallel robot, and hardware-in-the-loop simulation.

JUNWEI HAN was born in Shenyang, Liaoning, China, in 1965. He received the B.S., M.S., and Ph.D. degrees in fluid power transmission and control system from the Harbin Institute of Technology, China, in 1986, 1989, and 1992, respectively. Since1997, he has been a Professor of the School of Mechatronics Engineering, Harbin Institute of Technology. His research interests include electro-hydraulic servo control and the key technology of large shaking table and swing platform.

YU YANG was born in Shenyang, Liaoning, China, in 1980. He received the B.S., M.S., and Ph.D. degrees from the School of Mechatronics Engineering, Harbin Institute of Technology, China, in 2003, 2005, and 2010, respectively. He is a member of the Institute of Electrohydraulic Servo Simulation and Test System, Harbin Institute of Technology. His research interests include structure design and control strategy of the six degree of freedom system and the key technologies of flight simulator.

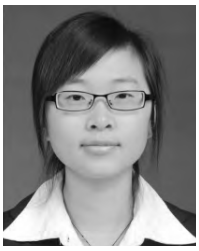

DONGMEI XU was born in Qingdao, Shandong, China, in 1987. She received the B.E. degree from the College of Mechanical and Electrical Engineering, Yantai University, China, in 2010, and the M.E. and Ph.D. degrees from the School of Mechatronics Engineering, Harbin Institute of Technology, China, in 2012 and 2018, respectively. She joined the School of Mechanical Engineering, Xi'an University of Science and Technology, where she has been a Lecturer since 2018. Her research interests include piezoelectric transducer, ultrasonic motor and ultra-precision piezoelectric actuating, and Stewart robot.

ZHIYONG QU was born in Yantai, Shandong, China, in 1978. He received the B.S., M.S., and Ph.D. degrees from the School of Mechatronics Engineering, Harbin Institute of Technology, China, in 1999, 2001, and 2006, respectively. He is currently an Associate Professor of the School of Mechatronics Engineering and also a member of the Institute of Electrohydraulic Servo Simulation and Test System, Harbin Institute of Technology. His research interests include modal analysis and control strategy of the redundant shaking table, structure design, and control strategy of the six degree of freedom system.